Progress In Electromagnetics Research B, Vol. 49, 429–455, 2013

GEOMETRICALLY LIT REGION ANALYSIS OF THE SINGLE-RAY DEBYE TERMS FOR THE TRANSMISSION OF A HIGH FREQUENCY PLANE WAVE INTO A DOUBLE-NEGATIVE CYLINDER BY THE MODIFIED WATSON TRANSFORMATION AND DEBYE SERIES EXPANSION

Saffet G. Şen*

Department of Electrical and Electronics Engineering, Atatürk University, Erzurum 25240, Turkey

Abstract—The Debye expansion integrals obtained by application of the Modified Watson Transformation and Debye series expansion to the Mie series for the high frequency plane wave transmitted into a double negative (DNG) cylinder are solved in the geometrically lit regions of the corresponding Debye series terms. The Debye series expansion is made up to the possible maximum term after which double ray field formation is first observed. Using the steepest descent method and the geometrical optics approximation, the role of the lower ray in the double-ray field formation is pointed out. For refractive indices satisfying $|n| \geq 10$, it is shown that the maximum Debye series term index up to which simple single-ray tracing can be performed is bigger for a DNG cylinder than that for a DPS cylinder and the difference between the term indices increases as $|n|$ increases.

1. INTRODUCTION

Double-negative (DNG) or left-handed (LH) metamaterials are artificial materials which exhibit a negative permittivity and a negative permeability simultaneously over a specific frequency range. These metamaterials were first introduced in [1] in 1968 by Veselago. The fundamentals of the physical realization of DNG metamaterials using split ring resonators and thin wires are presented in [2, 3]. In [4, 5], the construction of a DNG metamaterial and the experimental verification

Received 29 January 2013, Accepted 15 March 2013, Scheduled 19 March 2013

* Corresponding author: Saffet Gökçen Şen (gokcen.sen@atauni.edu.tr).

of the double-negativeness are reported. Recently proposed new structures for DNG metamaterials are presented in the references from [6] to [9]. Some recent applications of DNG metamaterials are given in the references from [10] to [14].

The transmission of a high frequency plane wave into a DNG infinitely long cylinder can be expressed using Mie series. However, Mie series does not reveal the physical mechanisms of the transmission process. In addition, the convergence speed of the Mie series can be a problem in some cases. In order to gain physical insight into the transmission process and overcome the convergence speed problem, the Modified Watson transform with Debye series expansion is applied to the Mie series. Watson transform was first used in [15]. Some other applications can be found in the references from [16] to [18]. Debye series expansion was first used in [19]. More instances of the Debye series expansion applications can be located in the references from [20] to [25].

The aim of this article is to examine the high frequency transmission into the DNG cylinder regions geometrically lit by only a single ray. The examination is made up to the maximum Debye series term after which double ray field formation is first observed. The differences between a DNG cylinder and a double positive cylinder are pointed out. The article is in some sense a continuation of [26].

As to the outline of the article, in the Section 2, the electromagnetic problem is defined and the Mie series solution is given. In the Section 3, the physical picture for the single-ray field formation is drawn for a general Debye series term using the geometrical optics (GO) approximation and the steepest descent method. In the Section 4, the numerical results are provided to validate the physical picture of the single-ray field formation. The differences between a DNG cylinder and a DPS cylinder are indicated. The conclusions are presented in the Section 5.

2. PROBLEM DESCRIPTION

A double-negative (DNG) cylinder of infinite length is illuminated by a high frequency plane wave propagating in the $-x$ direction in the free space. The time harmonic dependence is assumed to be $e^{-j\omega t}$ where ω is the angular frequency. The problem geometry is shown in Figure 1. The electric field intensity vector of the incident plane wave is given as follows:

$$\vec{E}_i = \hat{a}_z e^{-jk_0 x} \tag{1}$$

k_0 is the wavenumber of the free space. If the Mie series expansions of the electric field intensity vectors of the incident and transmitted

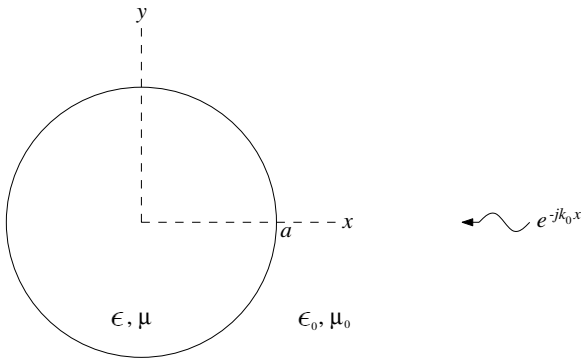

Figure 1. The problem geometry.

electromagnetic waves are carried out, then the following expressions are obtained:

$$\vec{E}_i = \hat{a}_z \sum_{l=-\infty}^{\infty} j^{-l} J_l(k_0\rho)\, e^{jl\phi} \tag{2}$$

$$\vec{E}_t = \hat{a}_z \sum_{l=-\infty}^{\infty} d_l J_l(nk_0\rho)\, e^{jl\phi} \tag{3}$$

j is equal to $\sqrt{-1}$ and n the refractive index of the DNG cylinder. $(\rho,\ \phi)$ is the cylindrical coordinates of the field point and d_l is the coefficient of the Mie series expansion for the transmitted field. The expression for d_l is given as follows:

$$d_l = j^{-l} \frac{\left[J_l(\beta)H_l^{(1)'}(\beta) - J_l'(\beta)H_l^{(1)}(\beta)\right]}{\left[J_l(\alpha)H_l^{(1)'}(\beta) - \frac{n}{\mu_r}J_l'(\alpha)H_l^{(1)}(\beta)\right]} \tag{4}$$

where

$$\beta = k_0 a \tag{5}$$

$$\alpha = n\beta \tag{6}$$

$f'(z_0)$ denotes differentiation with respect to the argument and is calculated as follows:

$$f'(z_0) = \left[\frac{df(z)}{dz}\right]_{z=z_0} \tag{7}$$

3. SINGLE-RAY DEBYE TERMS

A high frequency plane wave can be viewed as a collection of rays. Hence, the fields transmitted into the DNG cylinder can be thought to be the result of refracted and multiply reflected rays. This physical picture is shown in Figure 2. Each term of the Debye series matches with one of the rays shown in Figure 2. This physical picture is shown to be valid for the first term of the Debye series in [26]. The validation is to be generalized to the Debye series term of possible maximum index after which double ray field formation is first observed. It will be shown in the related part of this article that after a certain Debye series term index, the field in the geometrically lit region is formed by two rays.

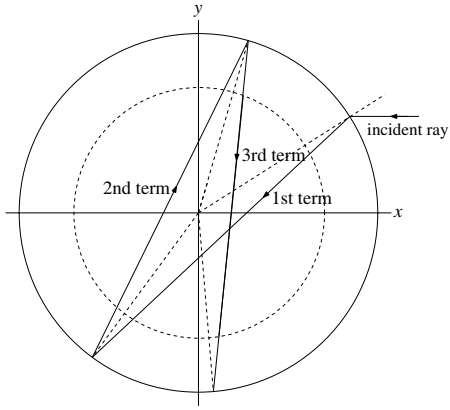

Figure 2. The physical picture of the transmission in a DNG cylinder.

Due to the detailed derivations and discussions in [26], the integral for the qth term of the Debye series can be written for the DNG cylinder as follows:

$$E_{t_q} = \frac{1}{2}\int_{-\infty+j\varepsilon}^{\infty+j\varepsilon}\left[e^{-jv2\pi q}e^{-jv\left(\phi-\frac{3\pi}{2}\right)}+e^{jv\left(\phi-\frac{\pi}{2}\right)}\right]T_{21}\frac{H_v^{(2)}(\beta)}{H_v^{(1)}(|\alpha|)}$$
$$\left[R_{11}\frac{H_v^{(2)}(|\alpha|)}{H_v^{(1)}(|\alpha|)}\right]^{q-1}H_v^{(2)}(|nk_0\rho|)dv+\frac{1}{2}\int_{-\infty+j\varepsilon}^{\infty+j\varepsilon}\left[e^{-jv2\pi(q-1)}e^{-jv\left(\phi-\frac{3\pi}{2}\right)}\right.$$
$$\left.+e^{jv\left(\phi-\frac{\pi}{2}\right)}\right]T_{21}\frac{H_v^{(2)}(\beta)}{H_v^{(1)}(|\alpha|)}\left[R_{11}\frac{H_v^{(2)}(|\alpha|)}{H_v^{(1)}(|\alpha|)}\right]^{q-1}H_v^{(1)}(|nk_0\rho|)dv \quad (8)$$

where

$$T_{21} = \frac{4j}{\pi\beta H_v^{(1)}(\beta)H_v^{(2)}(\beta)\left([1\ \beta] + \frac{|n|}{|\mu_r|}[1\ |\alpha|]\right)} \tag{9}$$

$$R_{11} = -\frac{[1\ \beta] + \frac{|n|}{|\mu_r|}[2\ |\alpha|]}{[1\ \beta] + \frac{|n|}{|\mu_r|}[1\ |\alpha|]} \tag{10}$$

T_{21} is the coefficient of transmission of the incoming cylindrical wave from the medium 2, i.e., the free space, to the medium 1, i.e., the DNG medium. R_{11} is the coefficient of reflection of the outgoing cylindrical wave from the boundary of the cylinder to the DNG medium. $[i\ x]$ $(i = 1, 2)$ notation is defined as follows:

$$[i\ x] = \frac{H_v^{(i)'}(x)}{H_v^{(i)}(x)} \quad (i = 1, 2) \tag{11}$$

Since the geometrical optics (GO) approximation is to be used for the physical interpretation of the transmission process in the geometrically lit region, the Debye approximation for Hankel functions is to be employed in the integrands in (8). The Debye approximations for Hankel functions are

$$H_v^{(1)}(z) \sim \left(\frac{2}{\pi}\right)^{\frac{1}{2}}\left(z^2-v^2\right)^{-\frac{1}{4}}\exp\left\{j\left[\left(z^2-v^2\right)^{\frac{1}{2}} - v\cos^{-1}\left(\frac{v}{z}\right) - \frac{\pi}{4}\right]\right\} \tag{12}$$

$$H_v^{(2)}(z) \sim \left(\frac{2}{\pi}\right)^{\frac{1}{2}}\left(z^2-v^2\right)^{-\frac{1}{4}}\exp\left\{-j\left[\left(z^2-v^2\right)^{\frac{1}{2}} - v\cos^{-1}\left(\frac{v}{z}\right) - \frac{\pi}{4}\right]\right\} \tag{13}$$

The Debye approximation of the second part of the integrand of the first integral in (8) is given by $A(v)\exp[f(v)]$ where

$$A(v) = \left(\frac{2}{\pi}\right)^{\frac{1}{2}} T_{21}R_{11}^{q-1}\frac{\left[(|n|k_0\rho)^2 - v^2\right]^{-\frac{1}{4}}\left(\beta^2 - v^2\right)^{-\frac{1}{4}}}{\left(|\alpha|^2 - v^2\right)^{-\frac{1}{4}}}e^{j(2q-1)\frac{\pi}{4}} \tag{14}$$

$$\begin{aligned} f(v) = {} & j\left[-\left(\beta^2 - v^2\right)^{\frac{1}{2}} + \left((|n|k_0\rho)^2 - v^2\right)^{\frac{1}{2}} - (2q-1)\left(|\alpha|^2 - v^2\right)^{\frac{1}{2}}\right] \\ & + jv\left[\cos^{-1}\left(\frac{v}{\beta}\right) - \cos^{-1}\left(\frac{v}{|n|k_0\rho}\right)\right. \\ & \left. + (2q-1)\cos^{-1}\left(\frac{v}{|\alpha|}\right) + \phi - \frac{\pi}{2}\right] \end{aligned} \tag{15}$$

The saddle point equation or the steepest descent equation is obtained from $f'(v) = 0$ as

$$j\left[\cos^{-1}\left(\frac{v}{\beta}\right) - \cos^{-1}\left(\frac{v}{|n|k_0\rho}\right) + (2q-1)\cos^{-1}\left(\frac{v}{|\alpha|}\right) + \phi - \frac{\pi}{2}\right] = 0 \quad (16)$$

If the variable transformation

$$v = \beta\sin(x) \quad (17)$$

is made in the saddle point equation, and the resulting equation is solved using a mathematical software like Mathematica, then it will be observed that x is the incidence angle of the upper ray that illuminates the field point after $q-1$ reflections. The verification of this fact can be performed in several other ways.

A geometrical relation between the incidence angle of the upper ray and the field point angle can be obtained from the physical picture in Figure 3. This relation is given for a general q as follows:

$$\theta + \cos^{-1}\left(\frac{\frac{a}{|n|}\sin\theta}{\rho}\right) - (2q-1)\cos^{-1}\left(\frac{\sin\theta}{|n|}\right) = \phi \quad (18)$$

In Figure 3, the dashed circle is called the field circle, i.e., the circle on which the field point resides.

If the variable transformation is used in the saddle point equation, then the following equation is obtained:

$$x + \cos^{-1}\left(\frac{\frac{a}{|n|}\sin x}{\rho}\right) - (2q-1)\cos^{-1}\left(\frac{\sin x}{|n|}\right) = \phi \quad (19)$$

If Equation (19) is compared with Equation (18), then x turns out to be the same as θ.

The upper ray incident on the point $P(a,\theta)$ has a phase of $-k_0 a\cos(\theta)$. After $q-1$ internal reflections, this phase must be summed with the phase contribution due to the total path taken by the ray according to the GO approximation. However, since the cylinder is DNG and the phase velocity is opposite to the power propagation direction, this phase contribution must be subtracted from the initial phase. Hence, it is expected that the steepest descent evaluation of the second part of the first integral contains this phase expression in agreement with the GO approximation. The steepest descent evaluation of the second part of the first integral is

$$\frac{1}{2}\left\{A(v)\exp[f(v)]\sqrt{\frac{-2\pi}{f''(v)}}\right\}_{v=\beta\sin(\theta)} \quad (20)$$

The phase of this expression is given by

$$\left[\left(\left(|n|k_0\rho\right)^2 - v^2\right)^{\frac{1}{2}} - (2q-1)\left(|\alpha|^2 - v^2\right)^{\frac{1}{2}}\right]_{v=\beta\sin(\theta)} - \beta\cos(\theta) \quad (21)$$

Before each internal reflection of the ray, a path of length

$$2\left[a^2 - \left(\frac{a}{n}\sin\theta\right)^2\right]^{\frac{1}{2}} \quad (22)$$

is taken by the ray. After the last internal reflection, a path of length

$$\left[a^2 - \left(\frac{a}{|n|}\sin\theta\right)^2\right]^{\frac{1}{2}} - \left[\rho^2 - \left(\frac{a}{|n|}\sin\theta\right)^2\right]^{\frac{1}{2}} \quad (23)$$

The total length of the path taken by the ray is given as

$$(2q-1)\left[a^2 - \left(\frac{a}{|n|}\sin\theta\right)^2\right]^{\frac{1}{2}} - \left[\rho^2 - \left(\frac{a}{|n|}\sin\theta\right)^2\right]^{\frac{1}{2}} \quad (24)$$

Then, according to the GO, the phase of the incident wave must take

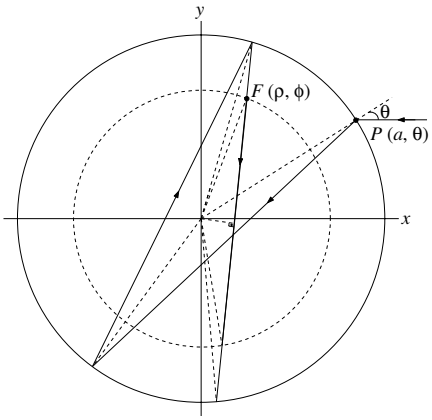

Figure 3. The physical picture of the transmission by the upper ray in a DNG cylinder for $q = 3$. The first intersection of the upper ray with the field circle for $q = 3$.

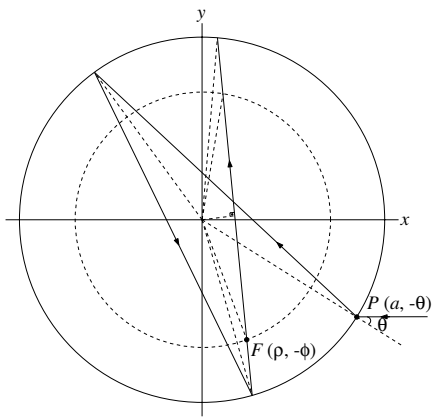

Figure 4. The physical picture of the transmission by the lower ray in a DNG cylinder for $q = 3$. The first intersection of the lower ray with the field circle for $q = 3$.

the following form:

$$-\beta\cos(\theta) - |n|k_0\left\{(2q-1)\left[a^2-\left(\frac{a}{|n|}\sin\theta\right)^2\right]^{\frac{1}{2}} - \left[\rho^2-\left(\frac{a}{|n|}\sin\theta\right)^2\right]^{\frac{1}{2}}\right\} \tag{25}$$

The expression in (25) is the same as the expression in (21). Hence, this is another verification for the fact that the ray of incidence angle θ forms the field at the point (ρ, ϕ). The amplitude verification of this fact is to be carried out numerically by comparing the steepest descent method (SDM) results with the Mie series results.

Now, the physical picture for the lower ray, i.e., the ray incident on the point $P(a, -\theta)$, is to be drawn and verified since the lower ray is critical in the field formation by two-rays. This field formation is represented by the first part of the integrand of the first integral in (8) and is shown in Figure 4.

For this case, the Debye approximation of the related integrand is to be made after using the following relation for the Hankel function of the second kind:

$$H_v^{(2)}(z) = e^{jv\pi}H_{-v}^{(2)}(z) \tag{26}$$

The Debye approximation is then made by replacing v by $-v$ in Equation (13). If the Debye approximation of the first part of the first integrand is denoted by $A(v)\exp[f(v)]$, then

$$A(v) = \left(\frac{2}{\pi}\right)^{\frac{1}{2}}\frac{\left(\beta^2-v^2\right)^{-\frac{1}{4}}\left(\left(|n|k_0\rho\right)^2-v^2\right)^{-\frac{1}{4}}}{\left(|\alpha|^2-v^2\right)^{-\frac{1}{4}}}T_{21}(R_{11})^{q-1}e^{j(2q-1)\frac{\pi}{4}} \tag{27}$$

$$\begin{aligned} f(v) = {} & j\left[-\left(\beta^2-v^2\right)^{\frac{1}{2}}+\left(\left(|n|k_0\rho\right)^2-v^2\right)^{\frac{1}{2}}-(2q-1)\left(|\alpha|^2-v^2\right)^{\frac{1}{2}}\right] \\ & +j(-v)\left[\cos^{-1}\left(\frac{-v}{\beta}\right)-\cos^{-1}\left(\frac{-v}{|n|k_0\rho}\right)\right. \\ & \left.+(2q-1)\cos^{-1}\left(\frac{-v}{|\alpha|}\right)+\phi-\frac{5\pi}{2}\right] \end{aligned} \tag{28}$$

The saddle point equation is obtained from $f'(v) = 0$ as follows:

$$\begin{aligned} & j(-1)\left[\cos^{-1}\left(\frac{-v}{\beta}\right)-\cos^{-1}\left(\frac{-v}{|n|k_0\rho}\right)\right. \\ & \left.+(2q-1)\cos^{-1}\left(\frac{-v}{|\alpha|}\right)+\phi-\frac{5\pi}{2}\right] = 0 \end{aligned} \tag{29}$$

Let the variable transformation

$$v = \beta \sin(-x) \tag{30}$$

be used in the saddle point equation to attain the following form:

$$-x - 2\pi - \cos^{-1}\left(\frac{\frac{a}{|n|}\sin x}{\rho}\right) + (2q-1)\cos^{-1}\left(\frac{\sin x}{|n|}\right) = -\phi \tag{31}$$

A geometrical relation can be obtained between the field point angle and the incidence angle of the lower ray for a general q using the physical picture in Figure 4 as follows:

$$-\theta - \cos^{-1}\left(\frac{\frac{a}{|n|}\sin\theta}{\rho}\right) + (2q-1)\cos^{-1}\left(\frac{\sin\theta}{|n|}\right) = -\phi \tag{32}$$

If Equations (31) and (32) are compared to each other, then it can be determined that

$$x = \theta - 2\pi \tag{33}$$

This means that the field at the point $F(\rho, -\phi)$ is formed by the lower ray of the incidence angle $-\theta$.

The phase of the steepest descent evaluation of the integral corresponding to the lower ray is

$$\left[\left((|n|k_0\rho)^2 - v^2\right)^{\frac{1}{2}} - (2q-1)\left(|\alpha|^2 - v^2\right)^{\frac{1}{2}}\right]_{v=\beta\sin(-\theta)} - \beta\cos(\theta) \tag{34}$$

Before arriving at the field point, the lower ray takes the path of the same length as the upper ray. Hence, the total phase of the lower ray at the field point is given by Equation (25) which is the same as the expression in (34). Hence, the field formation at the point $F(\rho, -\phi)$ is verified from the phase viewpoint.

Up to this point, the physical picture for the first part of the integral in (8) which contains the $H_v^{(2)}(|n|k_0\rho)$ function has been drawn. It has been observed that this integral represents the field formation as a result of the first intersection of a ray with the field circle. From another point of view, this ray is an incoming ray. It is time to describe the field formation mechanism for the second part of the integral that has the $H_v^{(1)}(|n|k_0\rho)$ function.

The Debye approximation of the second part of the second integral in (8) is denoted by $A(v)\exp[f(v)]$ where

$$A(v) = \left(\frac{2}{\pi}\right)^{\frac{1}{2}} T_{21}R_{11}^{q-1}\frac{\left[(nk_0\rho)^2 - v^2\right]^{-\frac{1}{4}}\left(\beta^2 - v^2\right)^{-\frac{1}{4}}}{\left(\alpha^2 - v^2\right)^{-\frac{1}{4}}}e^{j(2q+1)\frac{\pi}{4}} \tag{35}$$

$$f(v) = j\left[-\left(\beta^2 - v^2\right)^{\frac{1}{2}} - \left(\left(|n|k_0\rho\right)^2 - v^2\right)^{\frac{1}{2}} - (2q-1)\left(|\alpha|^2 - v^2\right)^{\frac{1}{2}}\right] + jv\left[\cos^{-1}\left(\frac{v}{\beta}\right) + \cos^{-1}\left(\frac{v}{|n|k_0\rho}\right) + (2q-1)\cos^{-1}\left(\frac{v}{|\alpha|}\right) + \phi - \frac{\pi}{2}\right] \quad (36)$$

The saddle point equation, $f'(v) = 0$, is

$$j\left[\cos^{-1}\left(\frac{v}{\beta}\right) + \cos^{-1}\left(\frac{v}{|n|k_0\rho}\right) + (2q-1)\cos^{-1}\left(\frac{v}{|\alpha|}\right) + \phi - \frac{\pi}{2}\right] = 0 \quad (37)$$

Using the variable transformation $v = \beta\sin(x)$ in the saddle point equation yields the following form:

$$-x + \cos^{-1}\left(\frac{\frac{a}{|n|}\sin x}{\rho}\right) + (2q-1)\cos^{-1}\left(\frac{\sin x}{|n|}\right) = -\phi \quad (38)$$

From Figure 5, a geometrical relation between the upper ray incidence angle and the field angle can be derived as follows:

$$-\theta + \cos^{-1}\left(\frac{\frac{a}{|n|}\sin\theta}{\rho}\right) + (2q-1)\cos^{-1}\left(\frac{\sin\theta}{|n|}\right) = -\phi \quad (39)$$

If Equation (38) is compared to Equation (39), then it can be observed that $x = \theta$. Hence, the solution of the saddle point equation is the incidence angle of the upper ray.

The steepest descent evaluation of the integral has the following phase part:

$$\left[-\left(\left(|n|k_0\rho\right)^2 - v^2\right)^{\frac{1}{2}} - (2q-1)\left(|\alpha|^2 - v^2\right)^{\frac{1}{2}}\right]_{v=\beta\sin\theta} - \beta\cos(\theta) \quad (40)$$

The upper ray of phase $-\beta\cos\theta$ takes a path of length

$$2\left[a^2 - \left(\frac{a}{|n|}\sin\theta\right)^2\right]^{\frac{1}{2}} \quad (41)$$

before each internal reflection. After the last internal reflection, there is a path of length

$$\left[a^2 - \left(\frac{a}{|n|}\sin\theta\right)^2\right]^{\frac{1}{2}} + \left[\rho^2 - \left(\frac{a}{|n|}\sin\theta\right)^2\right]^{\frac{1}{2}} \quad (42)$$

to arrive at the field point. The total path length is then

$$(2q-1)\left[a^2-\left(\frac{a}{|n|}\sin\theta\right)^2\right]^{\frac{1}{2}}+\left[\rho^2-\left(\frac{a}{|n|}\sin\theta\right)^2\right]^{\frac{1}{2}} \tag{43}$$

According to the GO, the final phase of the ray must be as follows:

$$-\beta\cos(\theta)-|n|k_0\left\{(2q-1)\left[a^2-\left(\frac{a}{|n|}\sin\theta\right)^2\right]^{\frac{1}{2}}\right.$$
$$\left.+\left[\rho^2-\left(\frac{a}{|n|}\sin\theta\right)^2\right]^{\frac{1}{2}}\right\} \tag{44}$$

The expression in (40) is the same as the one in (44). Hence, the physical picture in Figure 5 is verified in terms of the phase. The amplitude verification will be made by comparing the steepest descent method results with the Mie series results.

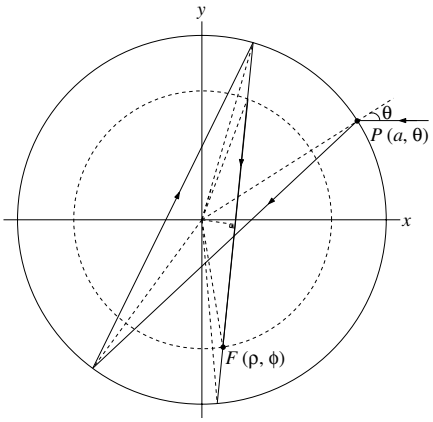

Figure 5. The physical picture of the transmission by the upper ray in a DNG cylinder for $q = 3$. The second intersection of the upper ray with the field circle for $q = 3$.

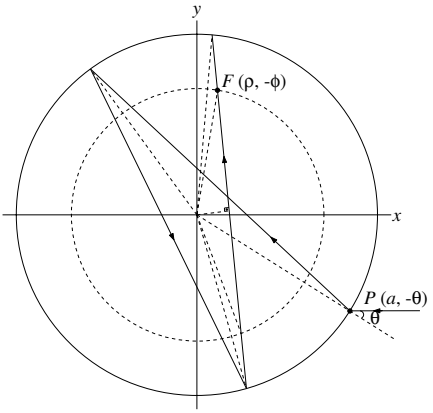

Figure 6. The physical picture of the transmission by the lower ray in a DNG cylinder for $q = 3$. The second intersection of the lower ray with the field circle for $q = 3$.

The physical picture shown in Figure 6 is to be proven now. The physical picture is related with the first part of the second integral in (8). After the application of the Debye approximation using the relation

$$H_v^{(1)}(z)=e^{-jv\pi}H_{-v}^{(1)}(z) \tag{45}$$

the integrand can be written as $A(v)\exp[f(v)]$ where

$$A(v)=\left(\frac{2}{\pi}\right)^{\frac{1}{2}}\frac{\left(\beta^2-v^2\right)^{-\frac{1}{4}}\left(\left(|n|k_0\rho\right)^2-v^2\right)^{-\frac{1}{4}}}{\left(|\alpha|^2-v^2\right)^{-\frac{1}{4}}}T_{21}(R_{11})^{q-1}e^{j(2q+1)\frac{\pi}{4}} \quad (46)$$

$$\begin{aligned}f(v)=j&\left[-\left(\beta^2-v^2\right)^{\frac{1}{2}}-\left(\left(|n|k_0\rho\right)^2-v^2\right)^{\frac{1}{2}}-(2q-1)\left(|\alpha|^2-v^2\right)^{\frac{1}{2}}\right]\\&+j(-v)\left[\cos^{-1}\left(\frac{-v}{\beta}\right)+\cos^{-1}\left(\frac{-v}{|n|k_0\rho}\right)\right.\\&\left.+(2q-1)\cos^{-1}\left(\frac{-v}{|\alpha|}\right)+\phi-\frac{5\pi}{2}\right] \quad (47)\end{aligned}$$

The saddle point equation is

$$\begin{aligned}&j(-1)\left[\cos^{-1}\left(\frac{-v}{\beta}\right)+\cos^{-1}\left(\frac{-v}{|n|k_0\rho}\right)\right.\\&\left.+(2q-1)\cos^{-1}\left(\frac{-v}{|\alpha|}\right)+\phi-\frac{5\pi}{2}\right]=0 \quad (48)\end{aligned}$$

The variable transformation $v=\beta\sin(-x)$ yields the following form for the saddle point equation:

$$-x-2\pi+\cos^{-1}\left(\frac{\frac{a}{|n|}\sin x}{\rho}\right)+(2q-1)\cos^{-1}\left(\frac{sin\theta}{|n|}\right)=-\phi \quad (49)$$

The geometrical relation between the field point angle and the ray incidence angle can be derived from Figure 6 as

$$-\theta+\cos^{-1}\left(\frac{\frac{a}{|n|}\sin\theta}{\rho}\right)+(2q-1)\cos^{-1}\left(\frac{\sin\theta}{|n|}\right)=-\phi \quad (50)$$

If Equation (48) is compared with Equation (49), then it can be determined that

$$x=\theta-2\pi \quad (51)$$

which means that the lower ray forms the field at the field point shown in Figure 6.

The phase of the steepest descent evaluation of the integral is

$$\left[-\left(\left(|n|k_0\rho\right)^2-v^2\right)^{\frac{1}{2}}-(2q-1)\left(|\alpha|^2-v^2\right)^{\frac{1}{2}}\right]_{v=\beta\sin\theta}-\beta\cos(\theta) \quad (52)$$

Before arriving at the field point, the lower ray takes the path of the same length as the upper ray. Hence, the total phase of the lower ray at the field point is given by Equation (44) which is the same as the expression in (51). Hence, the field formation at the point $F(\rho,-\phi)$ is verified from the phase viewpoint.

4. NUMERICAL RESULTS AND DISCUSSION

The Mie series results for the qth term of the Debye series of the transmitted field is given in [26] as follows:

$$E_{t_q} = \sum_{l=-\infty}^{\infty} \frac{j^{-l}}{2} e^{-jl2q\pi} T_{21} R_{11}^{q-1} \frac{H_l^{(2)}(\beta)}{H_l^{(1)}(|\alpha|)} \left[\frac{H_l^{(2)}(|\alpha|)}{H_l^{(1)}(|\alpha|)}\right]^{q-1} H_l^{(2)}(|n|k_0\rho)$$
$$+ \sum_{l=-\infty}^{\infty} \frac{j^{-l}}{2} e^{-jl(2q-2)\pi} T_{21} R_{11}^{q-1} \frac{H_l^{(2)}(\beta)}{H_l^{(1)}(|\alpha|)} \left[\frac{H_l^{(2)}(|\alpha|)}{H_l^{(1)}(|\alpha|)}\right]^{q-1} H_l^{(1)}(|n|k_0\rho) \quad (53)$$

The first series in (52) is compared to the steepest descent evaluation of the first integral in (8). The same comparison is performed between the second series in (52) and the steepest descent evaluation of the second integral in (8). The results of these comparisons are displayed for the following parameters:

$$\begin{aligned} n &= 10 \\ \beta &= 50\pi \\ |n|k_0\rho &= \frac{29}{38} \end{aligned} \quad (54)$$

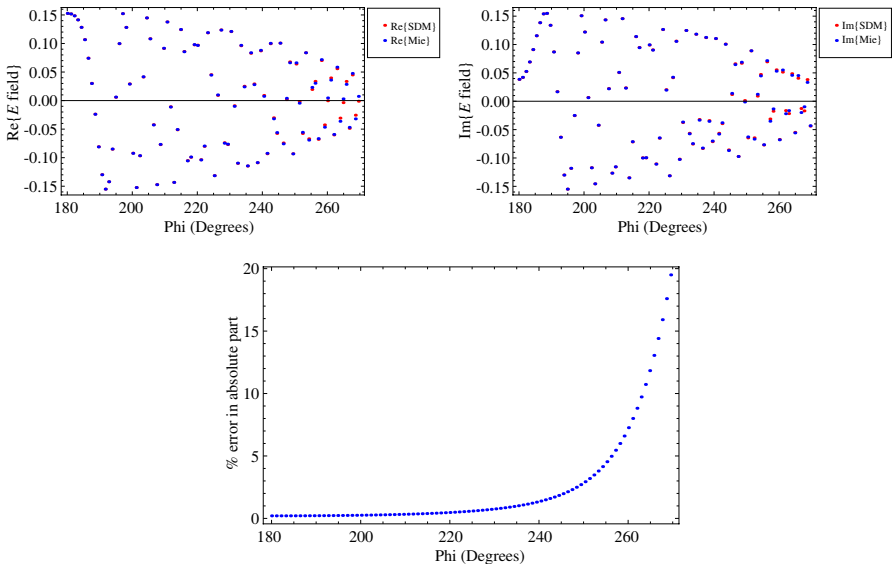

Figure 7. Mie series versus SDM, first intersection, $q = 2$.

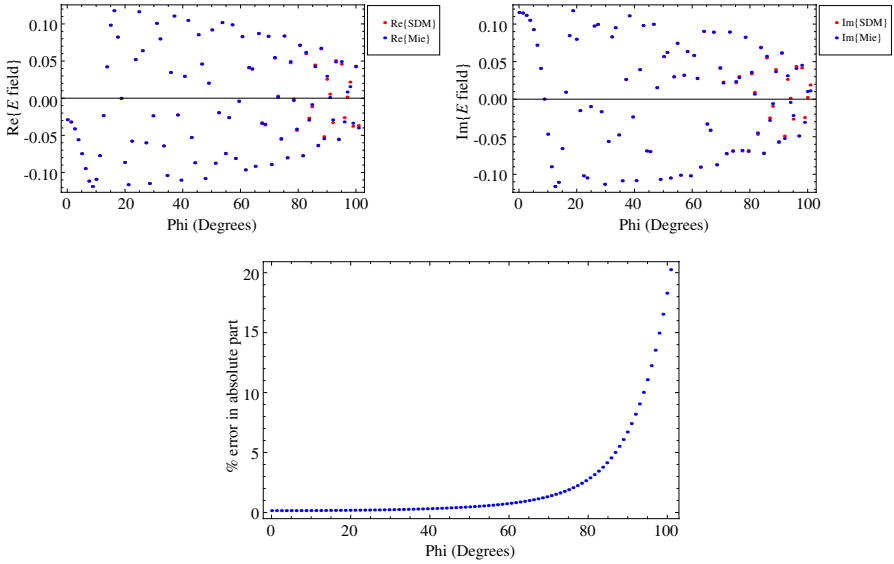

Figure 8. Mie series versus SDM, first intersection, $q = 3$.

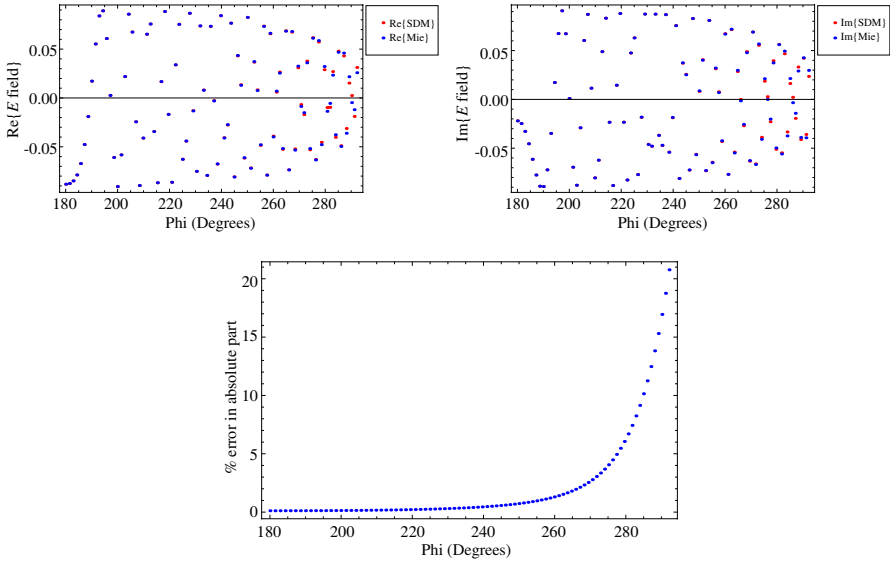

Figure 9. Mie series versus SDM, first intersection, $q = 4$.

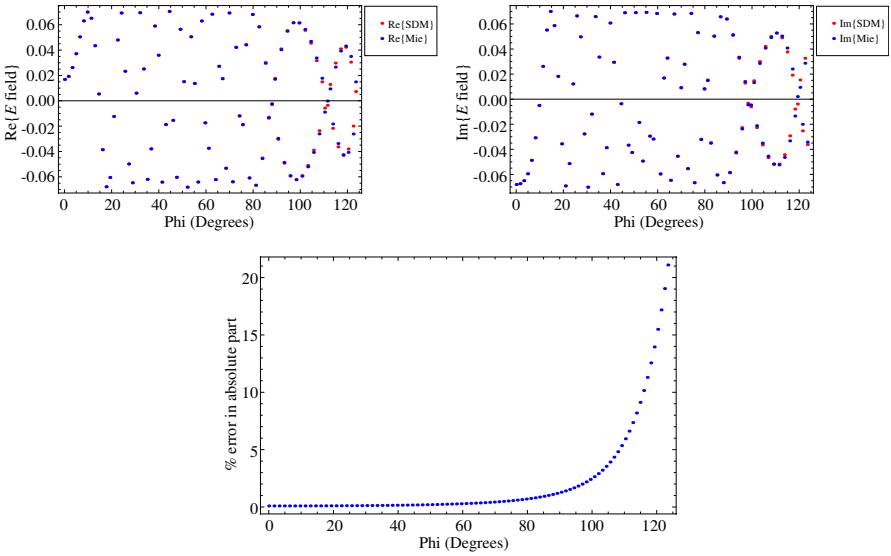

Figure 10. Mie series versus SDM, first intersection, $q = 5$.

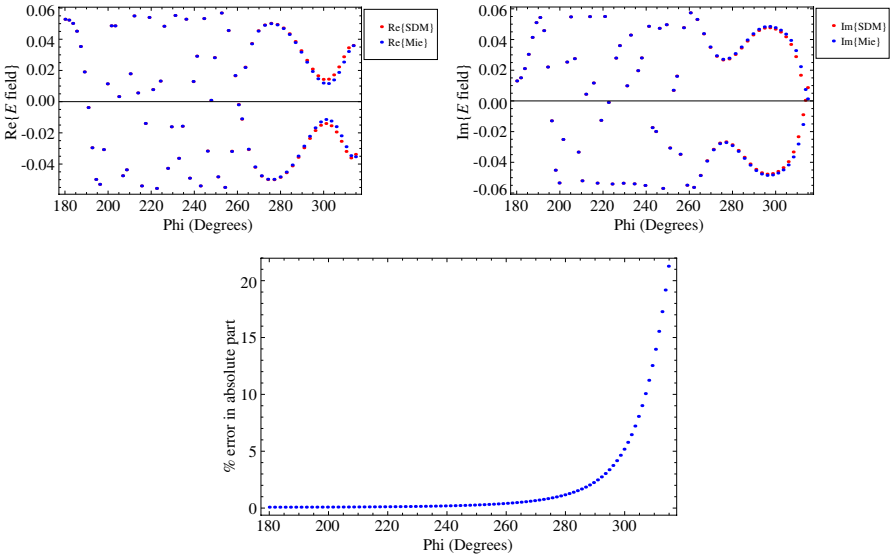

Figure 11. Mie series versus SDM, first intersection, $q = 6$.

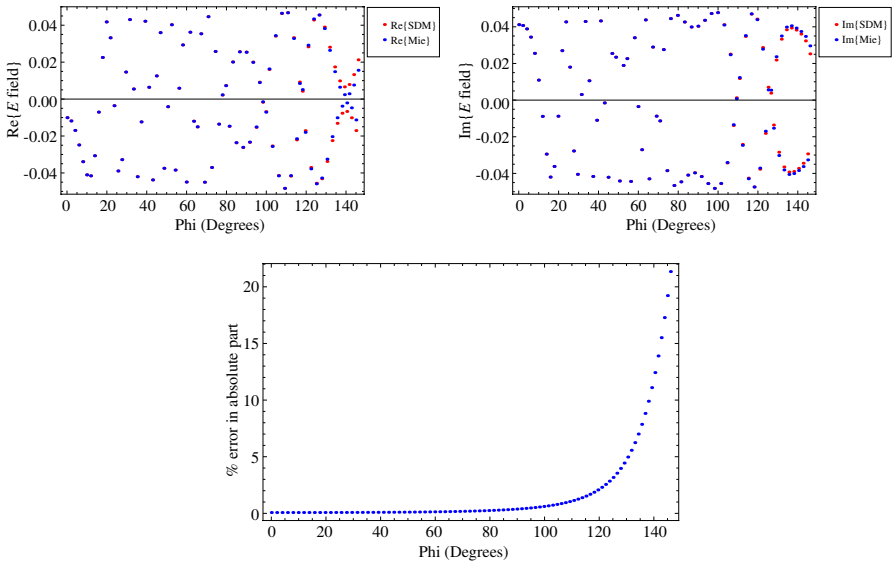

Figure 12. Mie series versus SDM, first intersection, $q = 7$.

The percentage (%) error is defined as follows:

$$\%\,\text{error} = \frac{|\text{Mie series result} - \text{SDM result}|}{|\text{Mie series result}|} \tag{55}$$

The figures from Figures 7 to 15 show that the Mie series results are in good agreement with the SDM results in a certain range of q, the index of the Debye term. In this way, the amplitude verification of the physical picture for the first intersection is performed.

The physical picture breaks down when q becomes 10 for the first intersection results. The reason of this failure can be determined if the geometrical relation between the incidence angle and the field angle, i.e., Equation (18), is plotted in Figure 16 for q values up to 10. For $q = 10$, the field angle starts from 180°, monotonically increases to and crosses 360°, then stops at 10.6°. Remembering the role of the lower ray which is the field formation at the field point $F(\rho, -\phi)$ when the field point of the upper ray is $F(\rho, \phi)$ reveals the fact that the field points in the field angle range $[349.4°, 360°] \cap [0°, 10.6°]$ are actually illuminated by both the upper ray and the lower ray. Hence, the single-ray picture is not valid in the field angle range $[349.4°, 360°] \cap [0°, 10.6°]$ which is a double-ray region. The single-ray picture is not valid in the transition region from the single ray region to the double ray region either. In these two regions, there is no agreement between the Mie

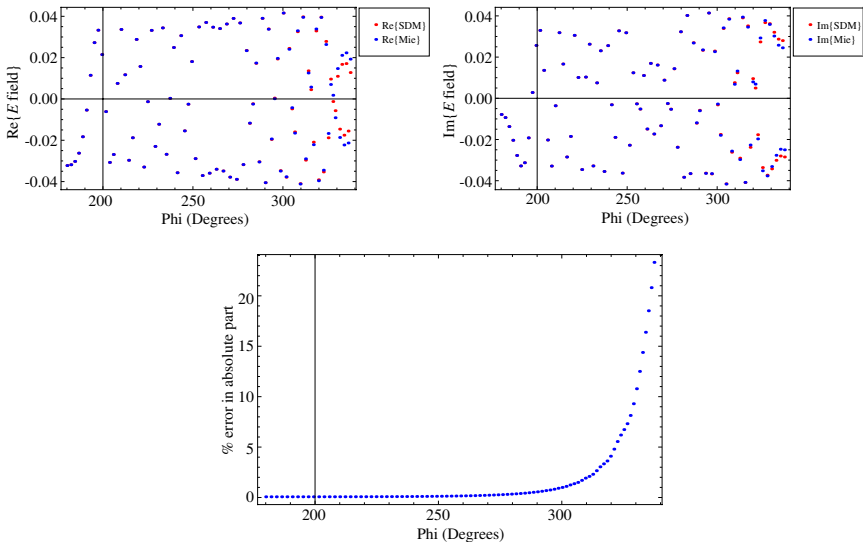

Figure 13. Mie series versus SDM, first intersection, $q = 8$.

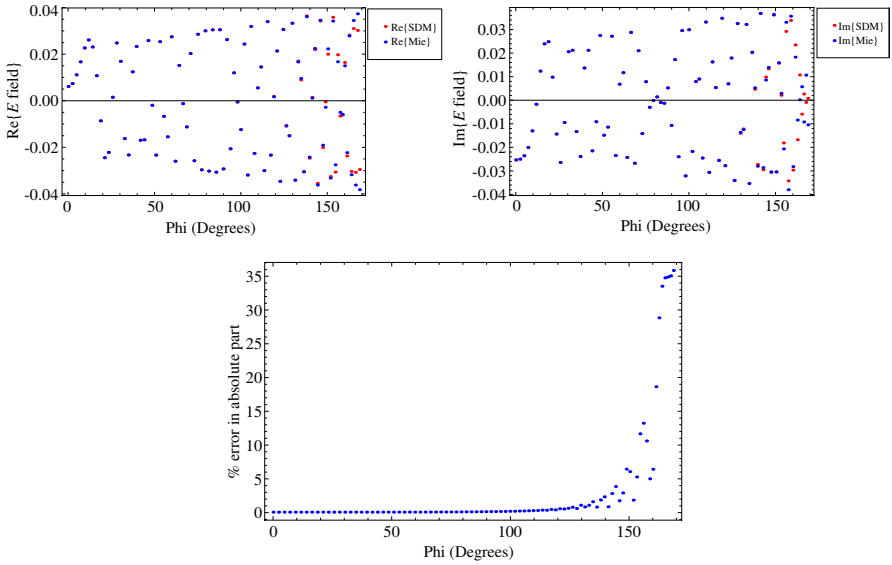

Figure 14. Mie series versus SDM, first intersection, $q = 9$.

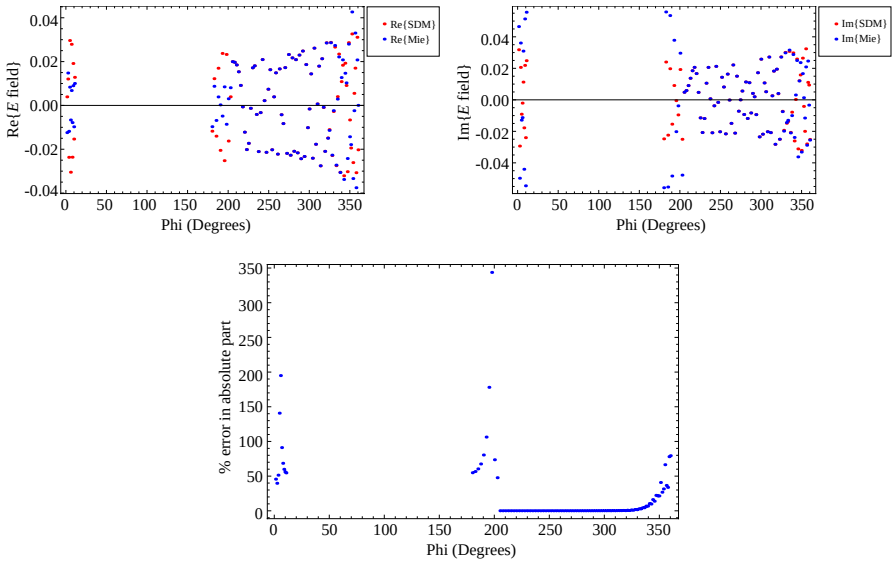

Figure 15. Mie series versus SDM, first intersection, $q = 10$.

Table 1. For large $|n|$ ($|n| \geq 10$), the inequalities satisfied by q values for which double-ray field formation first appears.

field point type	inequality satisfied by q
first intersection, DNG	(minimum even q) $> n\left(\frac{\pi}{4}\right) + \frac{1}{2}\frac{a}{\rho} + \frac{1}{2}$
second intersection, DNG	(minimum odd q) $> n\left(\frac{\pi}{4}\right) - \frac{1}{2}\frac{a}{\rho} + \frac{1}{2}$
first intersection, DPS	(minimum odd q) $> n\left(\frac{1}{2}\right) + \frac{1}{2}\frac{a}{\rho} + \frac{1}{2}$
second intersection, DPS	(minimum even q) $> n\left(\frac{1}{2}\right) - \frac{1}{2}\frac{a}{\rho} + \frac{1}{2}$

series results and the SDM results.

The figures from Figures 17 to 24 show that the Mie series results are in good agreement with the SDM results in a certain range of q, the index of the Debye term. In this way, the amplitude verification of the physical picture for the second intersection is performed. When q becomes equal to 9, the physical picture for the second intersection breaks down. If the plot of Equation (39) is examined for $q = 9$ in Figure 25, then it can be observed that the field angle starts from 180°, increases up to and crosses 360°, then stops at 14.17°. Due to the role of the lower ray in the field formation, the field angle range $[345.83°, 360°] \cap [0°, 14.17°]$ is a double-ray region. The single-ray

picture is not valid in the double ray region and the region of transition from the single-ray region to the double-ray region. Hence, in these angle ranges, the Mie series results and the SDM results do not agree with each other.

If the geometrical relation between the incidence angle and the field angle is analyzed, then some differences will be detected between a DNG cylinder and a DPS cylinder. In the Table 1, the minimum

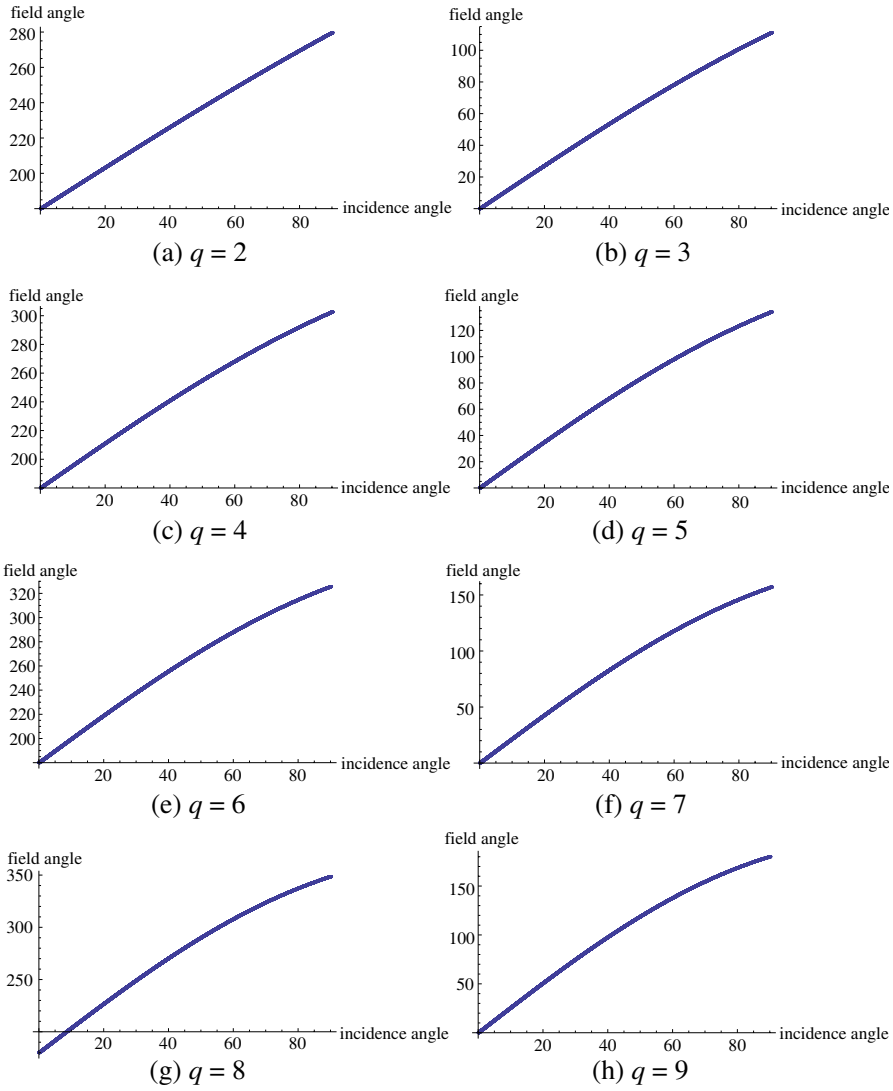

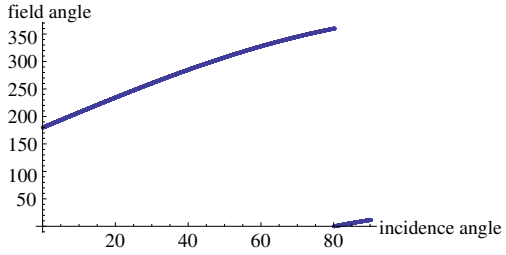

(i) $q = 10$

Figure 16. Incidence angle (degrees) versus field angle (degrees), first intersection.

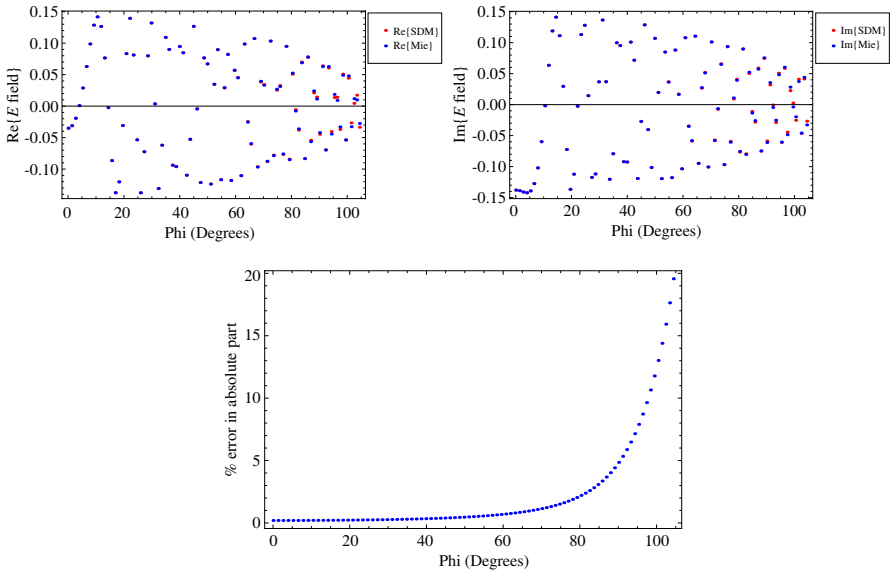

Figure 17. Mie series versus SDM, second intersection, $q = 2$.

q values for which the double-ray field formation appears first are tabulated for large $|n|$ ($|n| \geq 10$). If these relations are examined, then it can be determined that the q value for the first appearance of the double-ray field formation in a DNG cylinder is always larger than the q value for a DPS cylinder. In addition, the difference between the q value for a DNG cylinder and the q value for a DPS cylinder increases as $|n|$ increases. Hence, in a DNG cylinder, simple single-ray tracing can be performed for a longer range of q value.

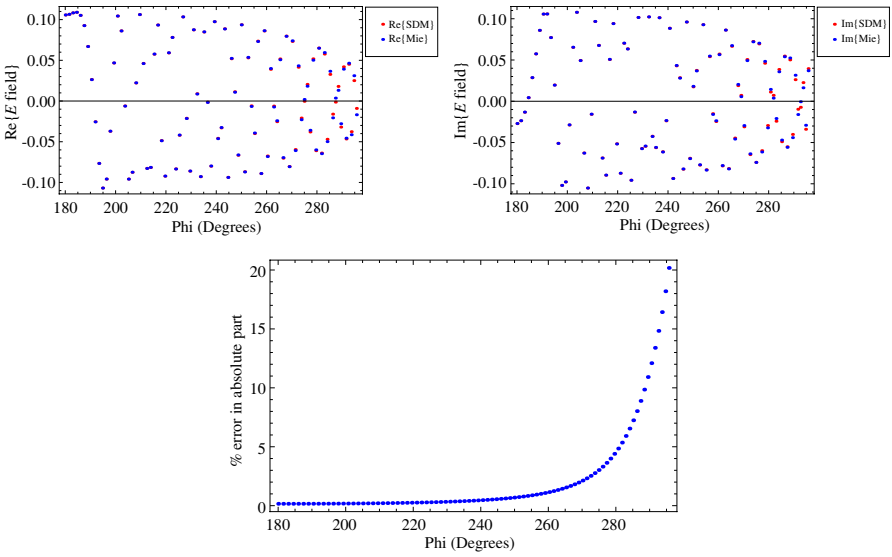

Figure 18. Mie series versus SDM, second intersection, $q = 3$.

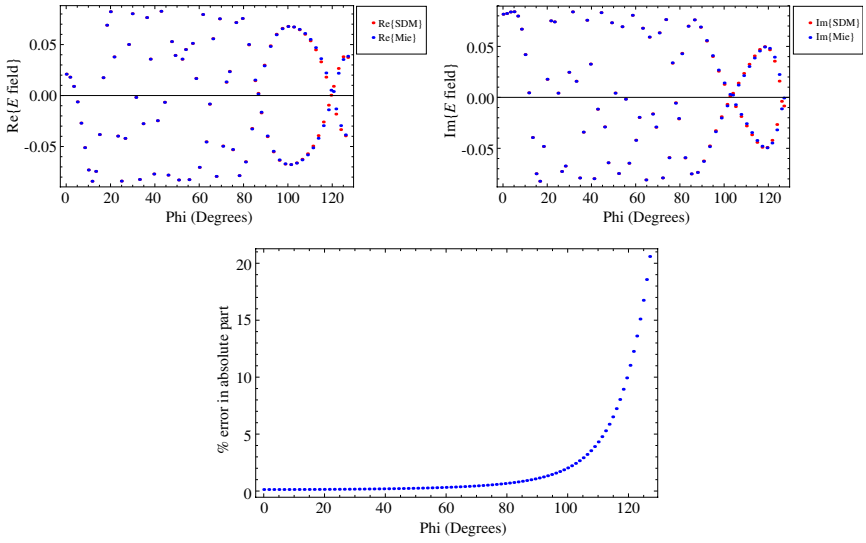

Figure 19. Mie series versus SDM, second intersection, $q = 4$.

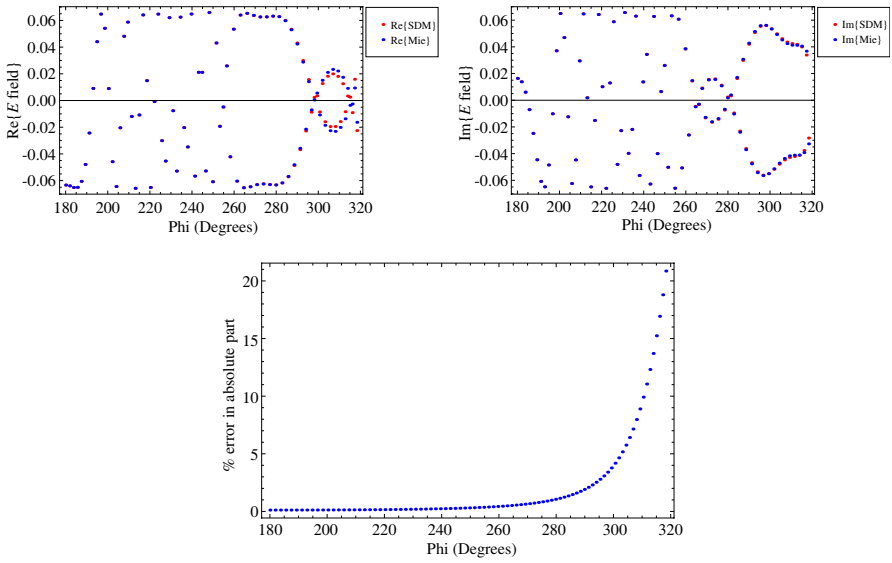

Figure 20. Mie series versus SDM, second intersection, $q = 5$.

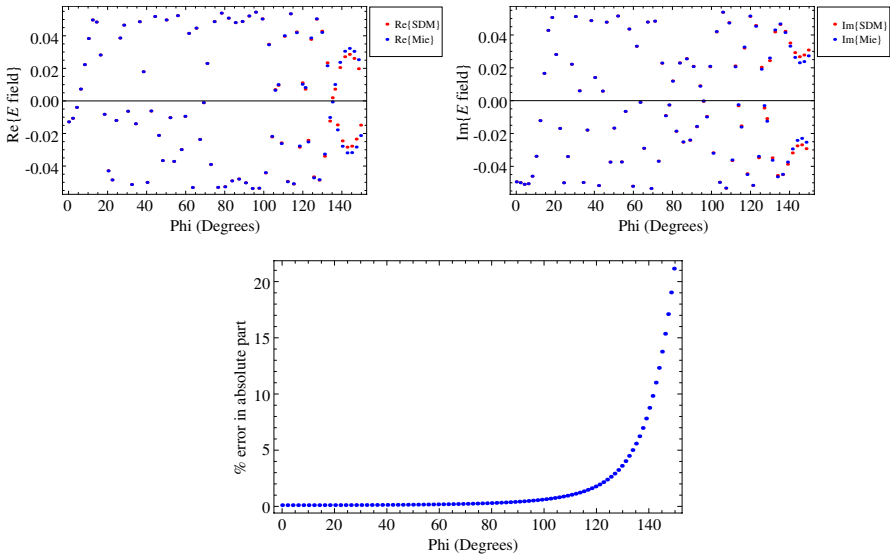

Figure 21. Mie series versus SDM, second intersection, $q = 6$.

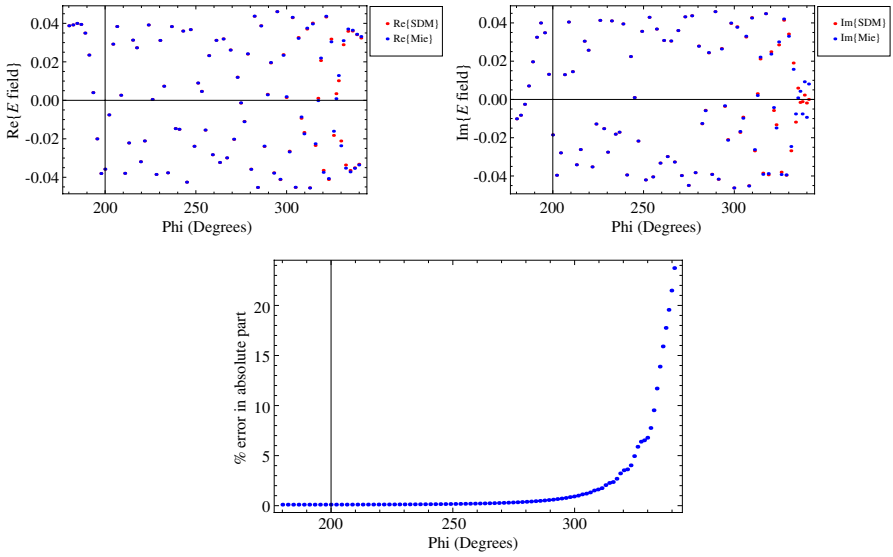

Figure 22. Mie series versus SDM, second intersection, $q = 7$.

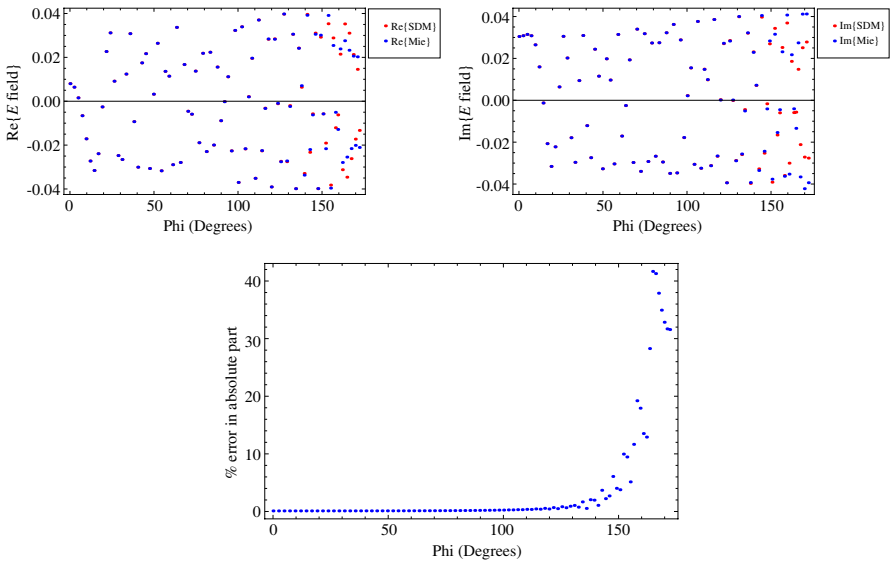

Figure 23. Mie series versus SDM, second intersection, $q = 8$.

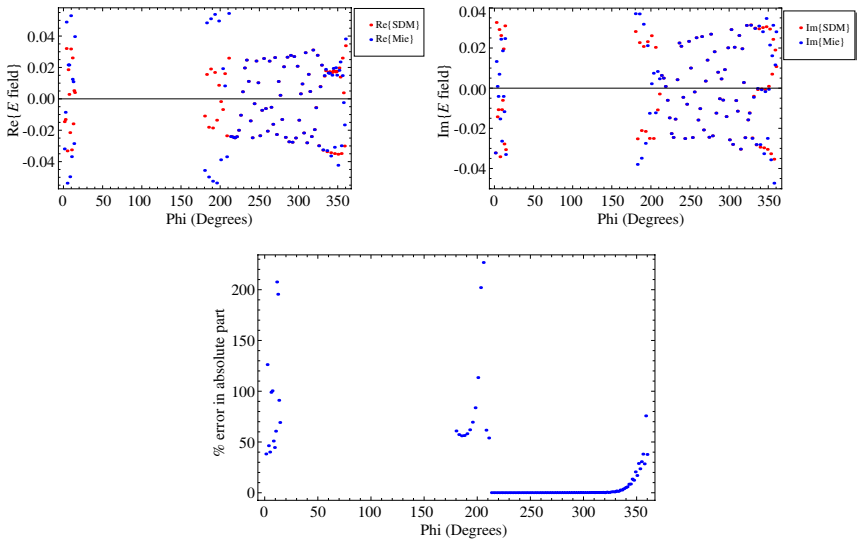

Figure 24. Mie series versus SDM, second intersection, $q = 9$.

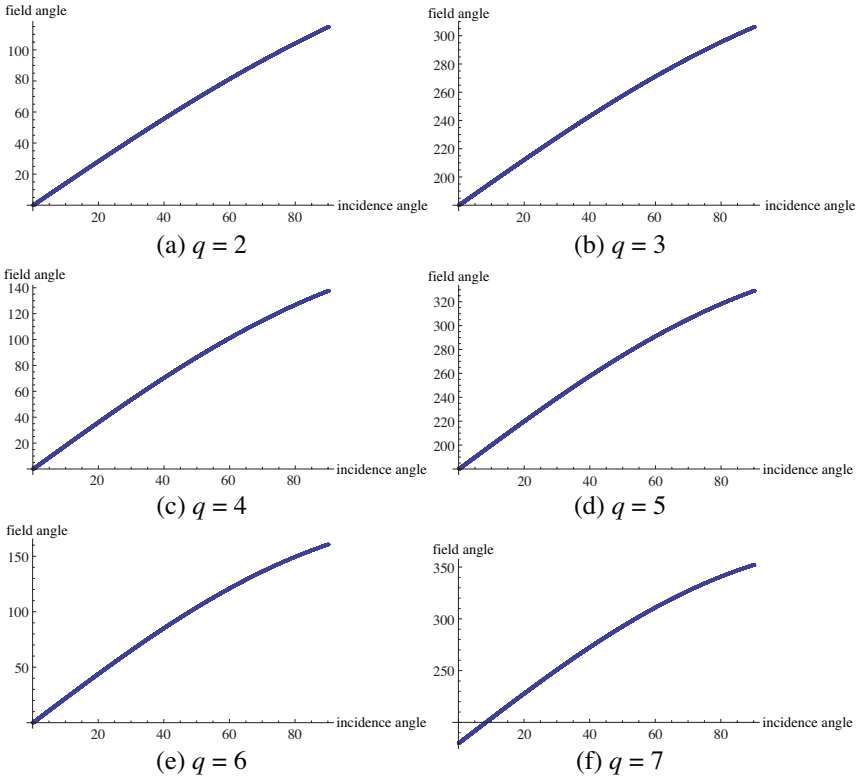

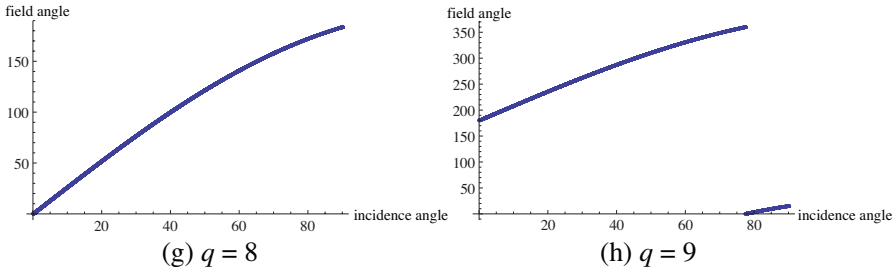

(g) $q = 8$ (h) $q = 9$

Figure 25. Incidence angle (degrees) versus field angle (degrees), second intersection.

5. CONCLUSION

By applying the modified Watson transformation to the Mie series for the transmitted field due to an incident high frequency plane wave and using the Debye series expansion in the resulting integral expression, the physical picture of the transmission process in the geometrically lit region has been drawn for the single-ray field formation. It has been proven that the field at $F(\rho, -\phi)$ is formed by a lower ray which is symmetric to the upper ray which establishes the field at the point $F(\rho, \phi)$. The role of the lower ray in the double-ray field formation has been explained. It has been shown for $|n| \geq 10$ that simple single-ray tracing can be carried out for a longer q range in a DNG cylinder than in a DPS cylinder. The fact that the difference between the range lengths increases as $|n|$ increases has also been stated.

REFERENCES

1. Veselago, V. G., "The electrodynamics of substances with simultaneously negative values of ϵ and μ," *Soviet Physics Uspekhi*, Vol. 10, No. 4, Jan.–Feb. 1968.
2. Pendry, J. B., A. J. Holden, D. J. Robbins, and W. J. Stewart, "Magnetism from conductors and enhanced nonlinear phenomena," *IEEE Transactions on Microwave Theory and Techniques*, Vol. 47, 2075–2084, Nov. 1999.
3. Pendry, J. B., A. J. Holden, W. J. Stewart, and I. Youngs, "Extremely low frequency plasmons in metallic mesostructures," *Physical Review Letters*, Vol. 76, 4773, Jun. 17, 1996.
4. Smith, D. R., W. J. Padilla, D. C. Vier, S. C. Nemat-Nasser, and S. Schultz, "Composite medium with simultaneously negative

permeability and permittivity," *Physical Review Letters*, Vol. 84, 4184, May 1, 2000.

5. Shelby, R. A., D. R. Smith, and S. Schultz, "Experimental verification of a negative index of refraction," *Science*, Vol. 292, Apr. 6, 2001.
6. Rahim, M. K. A., N. Ibrahim, H. A. Majid, et al., "Left-handed metamaterial structure incorporated with microstrip antenna," *Microwave and Optical Technology Letters*, Vol. 54, No. 12, 2828–2832, Dec. 2012.
7. Han, X., J.-S. Hong, D.-L. Jin, et al., "A novel structure for a broadband left-handed metamaterial," *Chinese Physics B*, Vol. 21, No. 9, Sep. 2012.
8. Wang, J., Z. Xu, B. Du, et al., "Achieving all-dielectric left-handed metamaterials via single-sized dielectric resonators," *Journal of Applied Physics*, Vol. 111, No. 4, Feb. 2012.
9. Sabah, C., "Novel, dual band, single and double negative metamaterials: Nonconcentric delta loop resonators," *Progress In Electromagnetics Research B*, Vol. 25, 225–239, 2010.
10. Mok, S., S. Kahng, and Y. Kim, "A wide band metamaterial ZOR antenna of a patch coupled to a ring mushroom," *Journal of Electromagnetic Waves and Applications*, Vol. 26, No. 13, 1667–1774, 2012.
11. Yoon, K.-C., J. H. Kim, and J.-C. Lee, "Band-pass filter with broad-side coupled triple split-ring resonator using left-handed metamaterial," *Microwave and Optical Technology Letters*, Vol. 53, No. 9, 2174–2177, Sep. 2011.
12. Alhawari, A. R. H., A. Ismail, M. A. Mahdi, et al., "Miniaturized ultra-wideband antenna using microstrip negative index metamaterial," *Electromagnetics*, Vol. 31, No. 6, 404–418, 2011.
13. Ng Mou Kehn, M., "Spherical slotted antenna coated with double layer of materials having combinations of singly and doubly negative parameters and consequences of mode resonances," *Progress In Electromagnetics Research B*, Vol. 45, 223–249, 2012.
14. Cojocaru, E., "Waveguides filled with bilayers of double-negative (DNG) and double-positive (DPS) metamaterials," *Progress In Electromagnetics Research B*, Vol. 32, 75–90, 2011.
15. Watson, G. N., "The diffraction of electric waves by the earth," *Proceedings of the Royal Society of London*, Vol. 95, No. 666, 83–99, 1918.
16. Li, M. K. and W. C. Chew, "A new Sommerfeld-Watson

transformation in 3-D," *IEEE Antennas and Wireless Propagation Letters*, Vol. 3, 75–78, Dec. 2004.

17. Valagiannopoulos, C. A., "An overview of the Watson transformation presented through a simple example," *Progress In Electromagnetics Research*, Vol. 75, 137–152, 2007.
18. Sha, W. E. I. and W. C. Chew, "High frequency scattering by an impenetrable sphere," *Progress In Electromagnetics Research*, Vol. 97, 291–325, 2009.
19. Debye, P., "Das elektromagnetische feld um ein zylinder und die theorie des regenbogens," *Physik. Z.*, Vol. 9, 775, 1908.
20. Ducasse, E. and M. Deschamps, "A nonstandard wave decomposition to ensure the convergence of Debye series for modelling wave propagation in an immersed anisotropic elastic plate," *Wave Motion*, Vol. 49, No. 8, 745–764, Dec. 2012.
21. Li, R., X. Han, and K. Ren, "Generalized Debye series expansion of electromagnetic plane wave scattering by an infinite multilayered cylinder at oblique incidence," *Physical Review E*, Vol. 79, No. 3, Mar. 2009.
22. Nussenzweig, H. M., "High-frequency scattering by an impenetrable sphere," *Annals of Physics*, Vol. 34, 23–95, 1965.
23. Nussenzweig, H. M., "High-frequency scattering by a transparent sphere. 1. Direct reflection and transmission," *Journal of Mathematical Physics*, Vol. 10, No. 1, 82–124, Jan. 1969.
24. Inada, H., "Diffracted field computations by a series expansion," *Radio Science*, Vol. 10, 205–220, Feb. 1975.
25. Şen, S. G. and M. Kuzuoğlu, "Analysis of high frequency plane wave scattering from a double negative cylinder via the modified Watson transformation and Debye expansion," *Progress In Electromagnetics Research*, Vol. 84, 55–92, 2008.
26. Şen, S. G., "Analysis of high frequency plane wave transmission into a double negative cylinder by the modified Watson transformation and Debye series expansion: First term of the Debye series," *Progress In Electromagnetics Research*, Vol. 112, 397–414, 2011.